UNIVERSITY
of
GLASGOW

Department of Physics & Astronomy
Experimental Particle Physics Group
Kelvin Building, University of Glasgow,
Glasgow, G12 8QQ, Scotland
Telephone: +44 (0)141 339 8855 Fax: +44 (0)141 330 5881

GLAS-PPE/98–03
27th June 1998

Highlights and Open Questions from ZEUS

Anthony T. Doyle[1)]
on behalf of the ZEUS Collaboration.

ABSTRACT

The latest results from the ZEUS experiment, as presented at the DIS98 workshop, are reviewed. A brief introduction to the status of the experiment is given. The review focuses on three areas: multi-scale problems in QCD including results on jets, charm, the dynamics of F_2 at low Q^2, forward jets and fragmentation functions; diffractive structure including results on Υ production, inclusive diffraction in DIS, event shapes and leading baryon production; and, the measurement and interpretation of the high-Q^2 neutral and charged current cross-sections.

Introductory talk presented at the DIS98 Workshop,
Brussels, April 1998.

Slides are available from
http://www-zeus.desy.de/conferences98/#dis98

---

[1] Alexander von Humboldt fellow (Hamburg II University), supported by DESY and PPARC.

HERA Progress: Since last year's DIS workshop, the data available for analysis at ZEUS has more than doubled, corresponding to an integrated luminosity from the 1994-97 data-taking periods of 46.6 pb^{-1}. This large data sample presents a significant challenge to the experimentalists in providing precise data in the many areas which HERA can uniquely access. The understanding of the ZEUS detector is being improved using the large data samples to calibrate in situ. To illustrate the current level of understanding of the detector: the integrated luminosity is currently known to better than $\pm 1.5\%$; the overall momentum scale of the central tracking detector has been established at below the 0.3% level following calibration using elastic J/ψ data; the electron energy scale in the barrel calorimeter has been calibrated to $\pm 1\%$ using DIS data; and, the hadronic energy scale has been determined within $\pm 3\%$ using DIS data and cross-checked using dijet events. Developments in the calibration of the detector, combined with the improved statistics, enable increasingly precise as well as new measurements to be performed, as discussed below.

1 Multi-Scale Problems in QCD

At HERA there is always at least one soft QCD scale, parameterised in terms of the parton densities of the proton which require input from data. Quantities are measured with an additional hard scale, such as the photon virtuality, Q^2, in inclusive F_2 measurements. The measurements are then compared to perturbative calculations where the cross-sections may be factorised and the soft input constrained. In general, an additional soft (hadronisation) scale enters wherever part of the hadronic final state is measured. In addition, in resolved photoproduction processes, the photon may also be described as a source of partons introducing an additional soft scale which again requires data input. An important point in the development of our understanding of QCD is to ensure that the measurements are well-defined theoretically at the required level of precision. These multi-scale measurements can then be confronted with the QCD predictions to test whether our current understanding is sufficient to describe the process under consideration. A wide range of measurements can be made at HERA which test our understanding of QCD and its factorisation properties.

Photon Structure:[1] Before discussing the latest preliminary measurements, it is worthwhile to note the uncertainties, as discussed in recently published results on inclusive jet production using the cone algorithm.[2] Experimentally the uncertainty on the jet energy scale of $\pm 3\%$ dominates the uncertainty on the cross-sections. Theoretically, the scale dependence on the renormalisation and factorisation scales varied between $E_T^{jet}/4 < \mu_F = \mu_R < E_T^{jet}$, is minimised for a cone radius $R \sim 0.6$, as observed earlier at the Tevatron. The variation of R_{sep}, the two-jet merging parameter, leads to similar uncertainties on the cross-section for $R < R_{sep} < 2R$. In order to minimise the theoretical uncertainties due to merging/seed-finding ambiguities, the iterative k_T-algorithm has been adopted. An inclusive dijet analysis was performed requiring $E_T^{jet_1} > 14$ GeV and $E_T^{jet_2} > 11$ GeV. At these E_T^{jet} values, comparisons with Monte Carlo indicate that multiple interactions (not included in the NLO calculations) are not required to describe the observed x_γ distributions or the jet profiles. To gain greater sensitivity to the internal structure of the photon the measurements are made at high-y ($0.5 < y < 0.85$), corresponding to the highest accessible photon energies. In Fig. 1 the $d\sigma/d\eta_2$ distribution for the second-highest energy jet is presented for fixed intervals of η_1. The shaded band represents the hadronic energy scale uncertainty. The hadronisation uncertainties have been estimated to be $\sim 10\%$, the scale uncertainties are estimated at $\sim 10\%$ while the proton parton densities are well constrained in the probed x region ($x \sim 10^{-2}$). The data are thus sensitive to the choice of photon parton densities, as illustrated by the comparison of the the data with the GS96 and GRV parameterisations. The ZEUS data has now reached a level of precision where the photon parton densities can be discriminated: a global analysis of photon parton densities incorporating such data is therefore required.

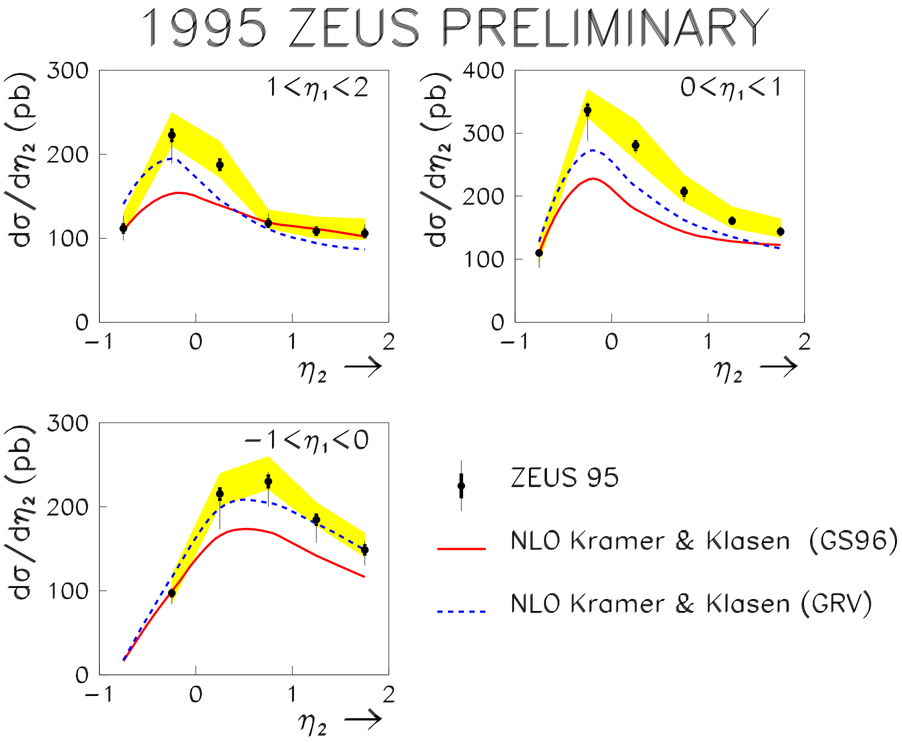

Fig. 1. Inclusive dijet photoproduction cross-sections.

Multijet Structure:[3] In order to probe the QCD matrix elements at a deeper level, an inclusive three-jet analysis has been performed using the k_T-algorithm for jets with $E_T^{jet} > 6$ GeV. The cross-section for such processes can be written as:

$$d\sigma(\gamma \mathsf{p} \rightarrow \mathsf{jjj}) = \sum \iint dx_\gamma dx_\mathsf{p} \underbrace{f_{1/\gamma}(x_\gamma) f_{2/\mathsf{p}}(x_\mathsf{p})}_{M^{\mathsf{jjj}}} \underbrace{|\mathcal{M}_{12\rightarrow 345}|^2}_{\cos\theta_3,\ \psi_3} \underbrace{dPS}_{X_3, X_4}$$

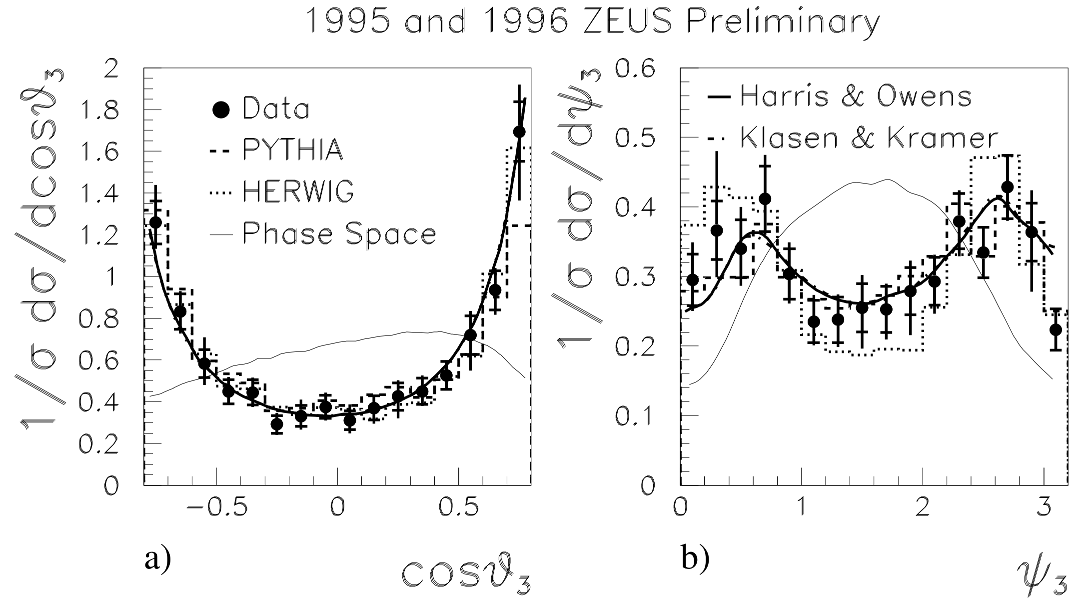

Fig. 2. Angular distributions for inclusive three-jet events compared to Monte Carlo simulations denoted by the histograms and the $\mathcal{O}(\alpha\alpha_S^2)$ calculations discussed in the text.

Here, the measured invariant mass distribution, M^{jjj}, is governed by the photon and proton parton densities, $f_{1/\gamma}(x_\gamma)$ and $f_{2/\mathsf{p}}(x_\mathsf{p})$, whereas the scaled energies of the jets, X_3 and X_4, are controlled largely by phase space. The measured angular distributions in the three-jet centre of mass are $\cos\theta_3$, where θ_3 is the angle the highest-energy jet makes w.r.t. the beam axis, and ψ_3, the angle of the three-jet plane w.r.t. the beam axis. The $\cos\theta_3$ distribution is determined by the spin of the primary exchange and the distribution of ψ_3 is related to the coherence property of the radiated (lowest-energy) jet to lie in the plane of the beam and the highest-energy jet. These are shown in Fig. 2, compared to $\mathcal{O}(\alpha\alpha_S^2)$ calculations (thick line) as well as to a phase space calculation (thin line) where the spin of the partons is ignored. The comparisons constitute a refined test of the photoproduction QCD matrix elements $\mathcal{M}_{12\rightarrow 345}$.

Charm in Photoproduction:[4] Heavy flavour production introduces a new scale with which to test perturbative QCD. Measurements of the $D^* \rightarrow (K\pi)\pi_s$ and $D^* \rightarrow (K\pi\pi\pi)\pi_s$ channels are shown to be in good agreement in Fig. 3(a). Two approaches have been taken in the

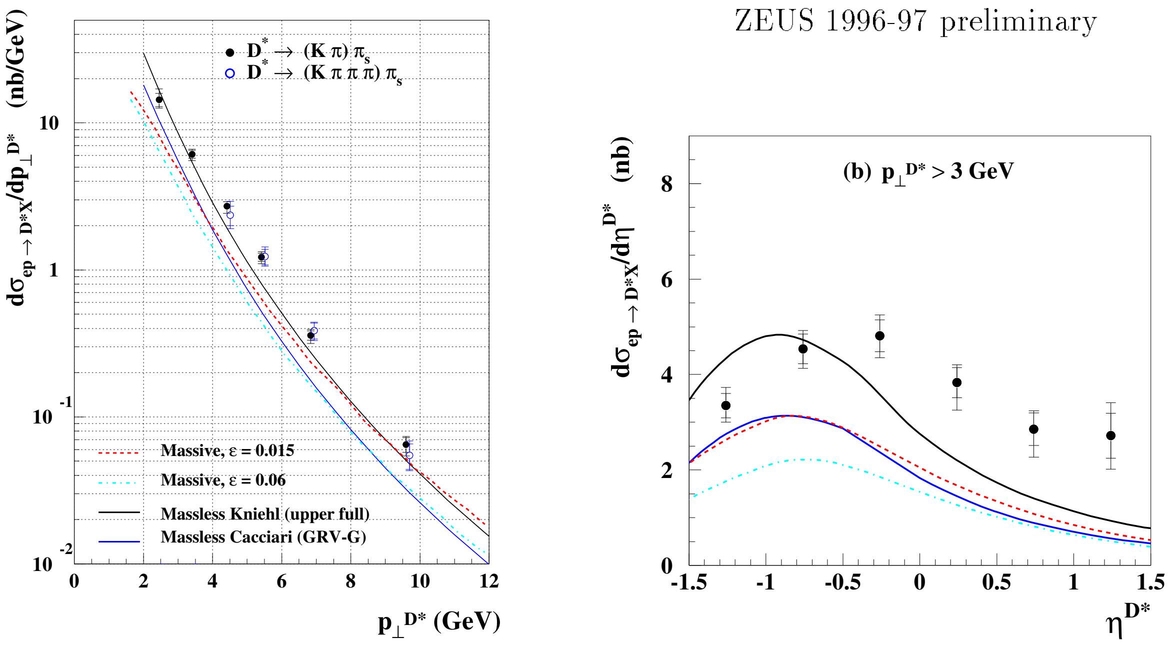

(a) D^* $p_\perp$ cross-section.

(b) $d\sigma/d\eta^{D^*}$ for $p_\perp > 3$ GeV.

Fig. 3. D^* ep cross-sections compared to NLO calculations.

calculations: the "massive" approach (dashed lines) where charm is generated dynamically and divergences are regulated by the charm mass; and the "massless" approach (full lines) where charm production is activated at the m_c threshold and massless approximations are used. Uncertainties arise due to the choice of the effective charm mass, and renormalisation and factorisation scales (here $\mu_R = \sqrt{m_c^2 + p_\perp^2} = \mu_F/2$) as well as the hardness of the charm decay to D^*, characterised in terms of ϵ_c in the Peterson fragmentation function for the "massive" calculations. The measured cross-section is typically underestimated in the calculations. In Fig. 3(b) this excess is observed to be predominantly in the forward direction. The open question is whether the data are more sensitive to the choice of input photon structure function or to the D^* fragmentation dynamics as we approach the proton fragmentation region or, perhaps, anomalously large contributions from $b \to c$ decays. Further information is provided by the measurement of associated dijets with $E_T^{jet_1} > 7$ GeV and $E_T^{jet_2} > 6$ GeV shown in Fig. 4. Here the measurement of x_γ^{OBS} has a relatively large contribution at low-x_γ whereas the "massive" NLO calculation is significantly more peaked towards one, underestimating the low-x_γ part of the cross-section. The question here is whether the dynamical generation of charm in photoproduction is sufficient, assuming that jet hadronisation effects, estimated at $\sim 10\%$ using Monte Carlo simulations, are relatively less important.

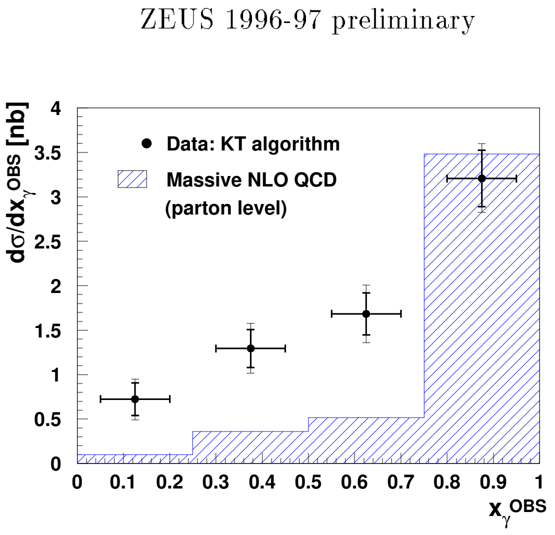

Fig. 4. D^*+dijet cross-section versus x_γ^{OBS}

Charm in DIS:[5] $D^* \rightarrow (K\pi)\pi_s$ measurements in DIS provide a significant test of the gluon density of the proton determined from the scaling violations of F_2. They will also help to constrain theoretical uncertainties in the fits to F_2 where different prescriptions for heavy flavour effects are adopted. Compared to the photoproduction case, they remove the uncertainty due to the choice of photon PDFs and hence reduce the number of open question posed above. The preliminary cross-section $\sigma^{ep\rightarrow D^*X} = 8.55 \pm 0.40^{+0.30}_{-0.24}$ nb is measured in the range $1 < Q^2 < 600$ GeV^2, $0.02 < y < 0.7, 1.5 < p_T(D^*) < 15$ GeV, and $\eta(D^*) < 1.5$. In Fig. 5, the upper plots show the measurements of the hadronic final state variables $p_T(D^*)$, $\eta(D^*)$ and x_{D^*}, the fractional momentum the D^* in the $\gamma^* p$ rest frame: the data agree with the massive NLO calculations where $\epsilon_c = 0.035$, except perhaps at lower x_{D^*} corresponding to higher $\eta(D^*)$. In addition the kinematic variables, W, Q^2 and x shown in the lower plots are in good agreement with the NLO calculations: it is therefore reasonable to extrapolate the measured cross-section to the full $\{\eta(D^*), p_T(D^*)\}$ range (1) to determine $F_2^c(x, Q^2)$ via the expression

$$\frac{d^2\sigma_{c\bar{c}X}}{dx\,dQ^2} = \frac{2\pi\alpha^2}{xQ^4}[(1 + (1-y)^2)F_2^c(x, Q^2) - y^2 F_L^c(x, Q^2)].$$

In Fig. 6, the $F_2^c(x, Q^2)$ data mirror the rise of F_2 at small x. The data are in agreement with the GRV94 PDFs, where the band represents an estimated theoretical uncertainty due to the effective charm mass ($m_c = 1.5 \pm 0.2$ GeV). This comparison verifies the steep rise of the gluon density at low x with a precision of $\simeq 15 - 20\%$.

---

[1] This procedure neglects the possibility of additional contributions outside the measured region due, for example, to intrinsic charm.

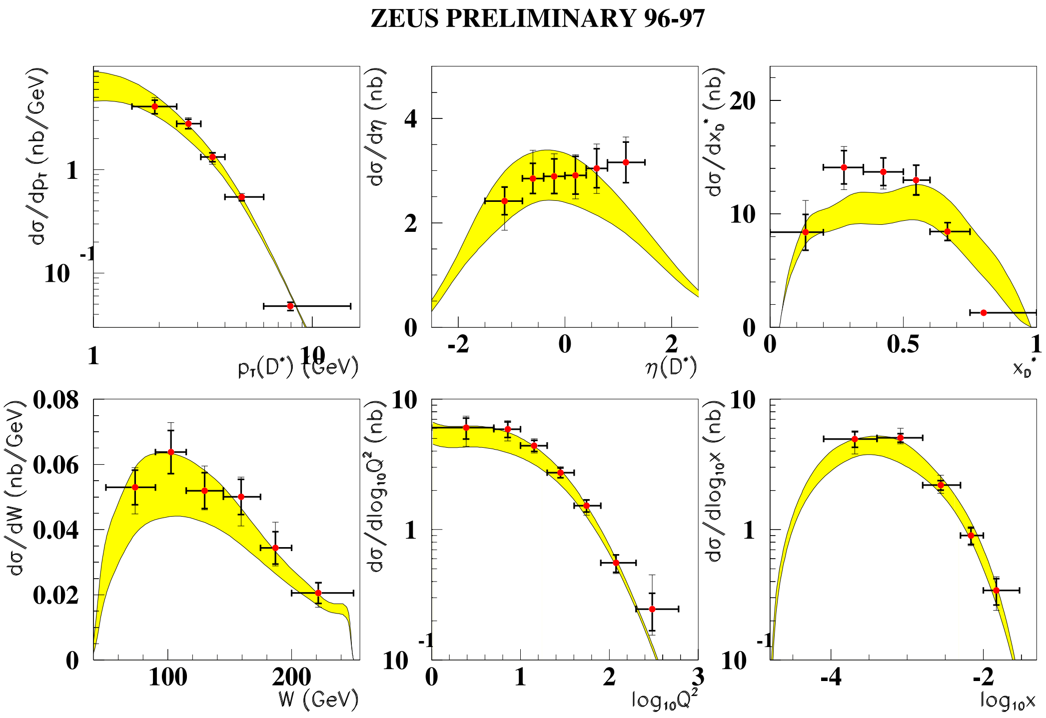

Fig. 5. DIS D^* cross-sections compared to NLO calculations (shaded band).

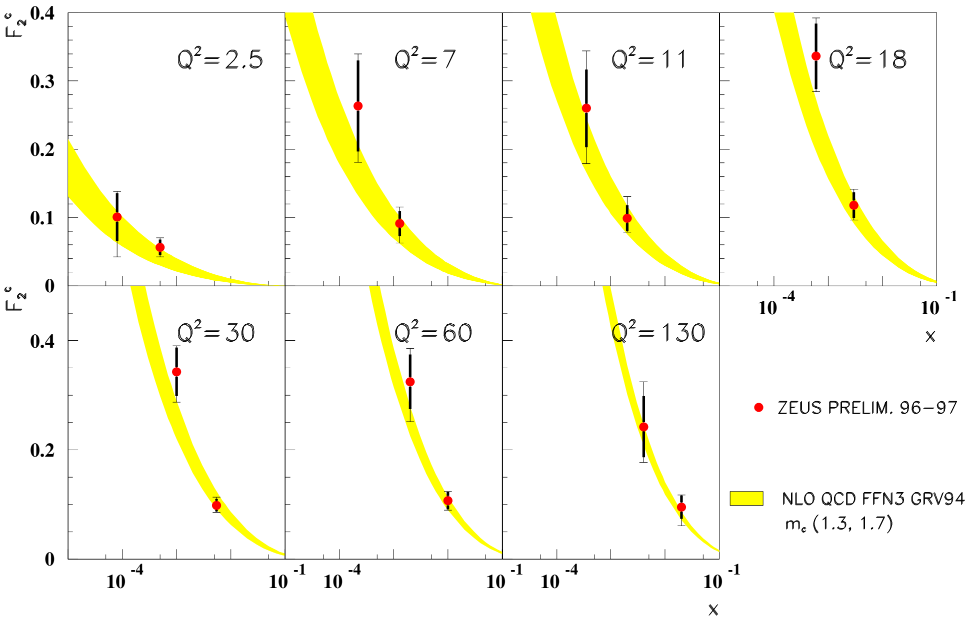

Fig. 6. $F_2^c(x, Q^2)$ as function of x for fixed Q^2 compared to NLO calculations.

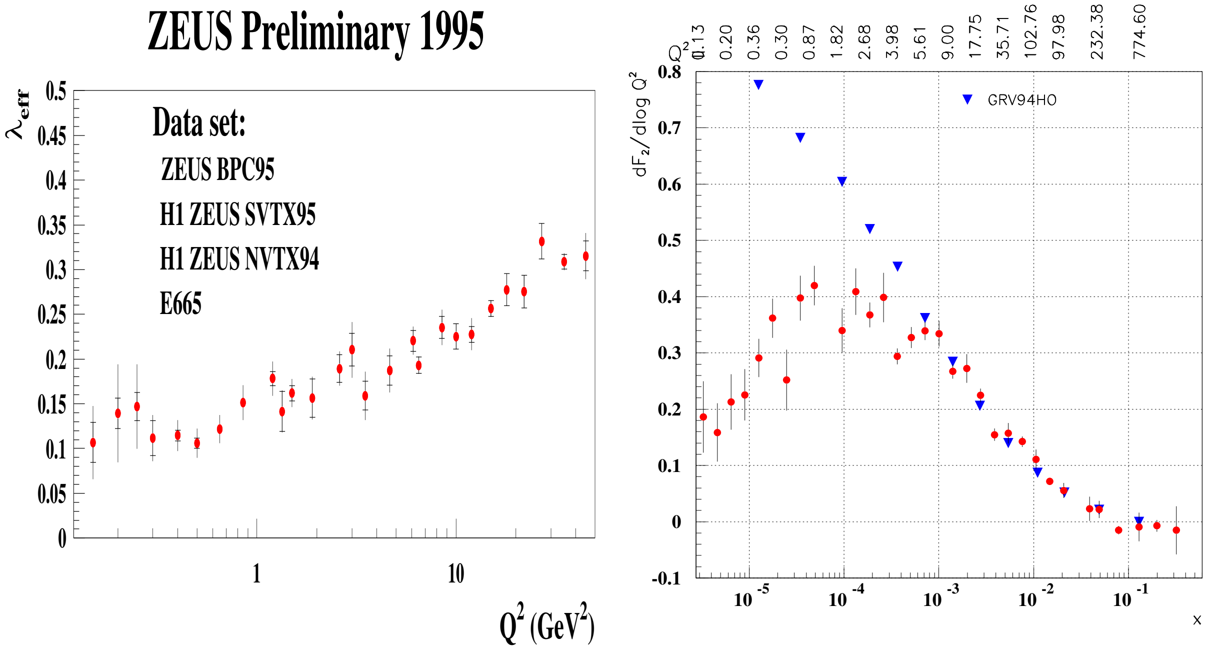

(a) $\lambda_{\rm eff}$ versus Q^2.

(b) $dF_2/dlogQ^2$ versus x.

Fig. 7. Fits to F_2 data (●) exploring the transition region.

Transition Region:[6] The corresponding rise of F_2 with decreasing x, or equivalently the rise of $\sigma^{tot}_{\gamma^\star p}$ with increasing W, has stimulated significant theoretical developments in the understanding of QCD at high energies. One challenge is to explore how and where the transition occurs from soft to hard physics and interpret low-Q^2 data. In order to relate the low-Q^2 and $Q^2 = 0$ data, a GVMD (Generalised Vector Meson Dominance) analysis has been performed. This analysis relates the virtual photon cross-section to the real cross-section via $\sigma^{tot}_{\gamma^\star p} = \sigma^{tot}_{\gamma p} \cdot M_0^2/(M_0^2 + Q^2)$, for fixed W (σ_L contributions at small Q^2 lead to a small correction of σ^{tot}). A good description of the ZEUS BPC data measured in the range $0.1 < Q^2 < 0.65$ GeV^2 is found with $M_0^2 = 0.53 \pm 0.04 \pm 0.10$ GeV^2. Extrapolating to $Q^2 = 0$ GeV^2, the corresponding $W^{2(\alpha_{I\!P}(0)-1)}$ dependence is given by the pomeron intercept value

$$\alpha_{I\!P}(0)_{BPC} = 1.145 \pm 0.02(stat) \pm 0.04(sys) \text{ (preliminary)}$$

to be compared with the Donnachie-Landshoff value $\alpha_{I\!P}(0) = 1.08$. In this Q^2 range, the rise of the cross-section is therefore relatively modest. This behaviour is also seen in the lower Q^2 points of Fig. 7(a). Here additional datsets are incorporated in fits to the F_2 data of the form $F_2 = c \cdot x^{\lambda_{\rm eff}} |_{Q^2}$. The parameter $\lambda_{\rm eff} \simeq \alpha_{I\!P}(0) - 1$ for $x < 0.01$ is then plotted as a function of Q^2. A relatively slow transition from $\lambda_{\rm eff} \simeq 0.1$ is observed with increasing Q^2. This rise of F_2 with decreasing x is intimately coupled to the scaling violations via the gluon density (in leading order $dF_2/dlogQ^2 \sim xg(x)$ neglecting sea quark contributions). In Fig. 7(b), fits of the form $F_2 = a + b \cdot log(Q^2)|_x$ have been performed to the published HERA data and the pre-HERA prediction from the GRV94 PDFs.[7] For $x \lesssim 10^{-4}$, corresponding to $< Q^2 > \lesssim 2$ GeV^2 there is a qualitative change in behaviour where the scaling violations stabilise and then decrease for lower-x values, a behaviour which is not reproduced by the GRV94 PDFs.

The question is whether this scaling violation behaviour and the slow onset of the rise of F_2 with decreasing x can be simultaneously understood. A DGLAP NLO fit to the $Q^2 > 1$ GeV^2 data (not shown) describes the data, demonstrating that there is sufficient flexibility in such an approach to go down to relatively low Q^2. However, the relatively stable scaling violations observed around $< Q^2 > \sim 2$ GeV^2 in Fig. 7(b) yield a gluon contribution which is rapidly diminishing at small-x and which is significantly smaller than the sea quark contribution for small starting scales, as illustrated in Fig. 8: in this low Q^2 region the sea appears to be driving the gluon at low-x. For larger Q^2 values the gluon dominates the sea and we have an intuitively appealing picture where gluons radiate sea quarks. Whether such low-Q^2 partons are universally valid could be tested using e.g. low-Q^2 F_2^c data.

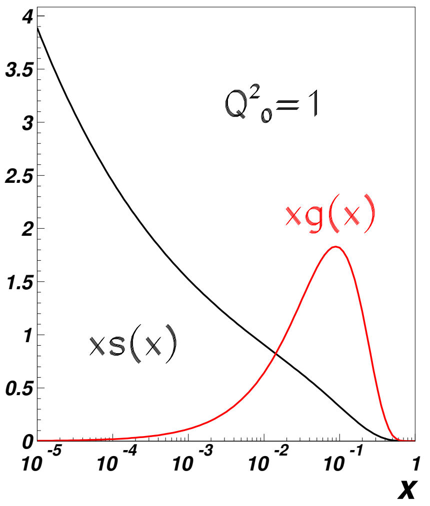

Fig. 8. Low Q^2 parton densities.

Forward Jet Production:[8] Why does F_2 rise? In the DGLAP approach the x dependence is an input determined at a starting scale Q_o^2 and evolved in Q^2. In the BFKL approach the x-dependence has recently been calculated in NLO. The underlying dynamics may be tested using semi-inclusive forward jet measurements in low-x events. Jets with $E_T^2 \sim Q^2$ and $x_{jet} \gtrsim x$, where x_{jet} is the momentum fraction of the jet relative to the incoming proton, are selected in order to enhance BFKL-like contributions where forward gluons may be emitted at relatively large E_T. In Fig. 9 the jets observed at detector level are shown as a function of E_T^2/Q^2 compared to three Monte Carlo simulations: LEPTO 6.5 and HERWIG 5.9 are DGLAP-based models such that gluons emitted at successively larger $x_{gluon} \sim x_{jet}$ have successively lower E_T whereas the colour dipole model ARIADNE 4.08 incorporates a BFKL feature that gluons are not strongly ordered. Three regions are identified: I - $E_T^2 < Q^2/2$, the "DGLAP" region, where all models approximately describe the data; II - $Q^2/2 < E_T^2 < 2Q^2$, the "BFKL" region where the DGLAP-based models (LEPTO 6.5 and HERWIG 5.9) fall below the data; and, III - $E_T^2 > 2Q^2$, where all models fail and we may need to describe the DIS data in terms of a virtual photon whose structure is being resolved by the high-E_T jets. The cross-section is evaluated in region II as a function of x for $x_{jet} > 0.036$ and $E_T > 5$ GeV in Fig. 10. BFKL dynamics leads to an enhancement of the forward jet production cross-section proportional to

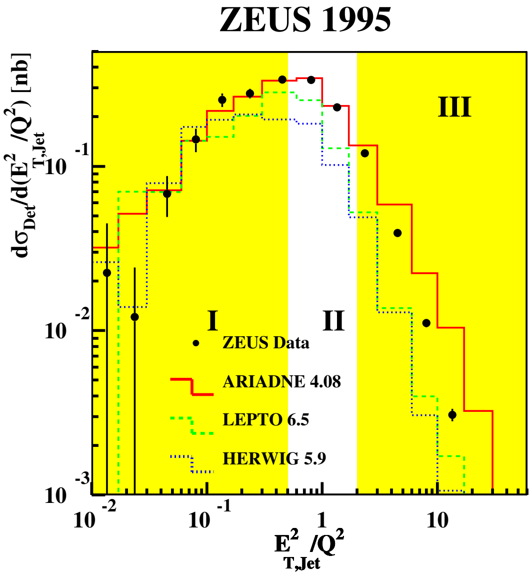

Fig. 9. Observed E_T^2/Q^2 distribution.

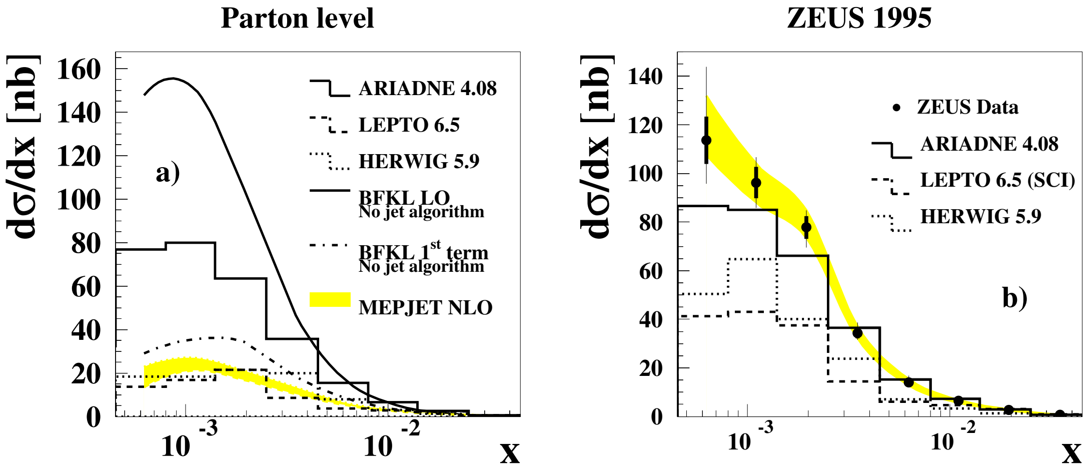

Fig. 10. Forward jet production cross-sections at (a) parton level and (b) hadron level. The data are compared to various predictions discussed in the text.

$(x_{jet}/x)^{\alpha_{I\!P}-1}$ over the $\mathcal{O}(\alpha\alpha_S^2)$ calculation. As shown in Fig. 10(a) there is a significant difference between the $\mathcal{O}(\alpha\alpha_S^2)$ MEPJET calculation (represented by the shaded band which includes the uncertainty on the renormalisation scale) compared to the leading-order BFKL prediction (full curve) at parton level. There are residual uncertainties in determining the hadron-to-parton level corrections and therefore the measurement in Fig. 10(b) is presented at hadron level. The rise of F_2 at small x is mirrored by the rise of the measured forward jet cross-section which is not described by the DGLAP-based models. A consistent description of the F_2 and forward-jet data represents a considerable challenge to our understanding of QCD.

Fragmentation Functions: Recently published results on jet shapes have shown that the observed patterns of QCD radiation in high-Q^2 neutral current and charged current are similar to those observed in e^+e^- experiments.[9] At HERA we are able to study these properties as a function of Q^2 in a single experiment and hence provide detailed information on quark fragmentation properties.[10] These properties can be studied in the semi-soft limit by measuring the $\ln(1/x_p)$ distributions, where $x_p = 2p/Q$ is the scaled momentum of charged hadrons in the current region of the Breit frame. The observed Gaussian distributions are then fitted within ± 1 of the mean to yield the $\ln(1/x_p)_{max}$ values as a function of Q given in Fig. 11(a). The precise data are consistent with data from e^+e^- experiments establishing the universality of fragmentation over a large range of Q. An MLLA+LPHD fit (indicated by the full line) of the form $\ln(1/x_p)_{max} = 1/2Y + c_2\sqrt{(Y)} - c_2^2$, where $Y = \ln Q/2\Lambda_{eff}$ and $c_2 = 0.52$ for three active flavours in the cascading process, provides a reasonable description of the data with $\Lambda_{eff} \simeq 245$ MeV. The high-statistics data enables the region of high x_p to be studied. In Fig. 11(b) the fragmentation function data are presented for different x_p intervals as a function of Q^2 (in various ranges of x). At high x_p and higher Q^2 the fragmentation functions exhibit negative scaling violations, consistent with a dominant QCD Compton process (c.f. high-x structure function data). The DIS data (full symbols) are observed to be reasonably

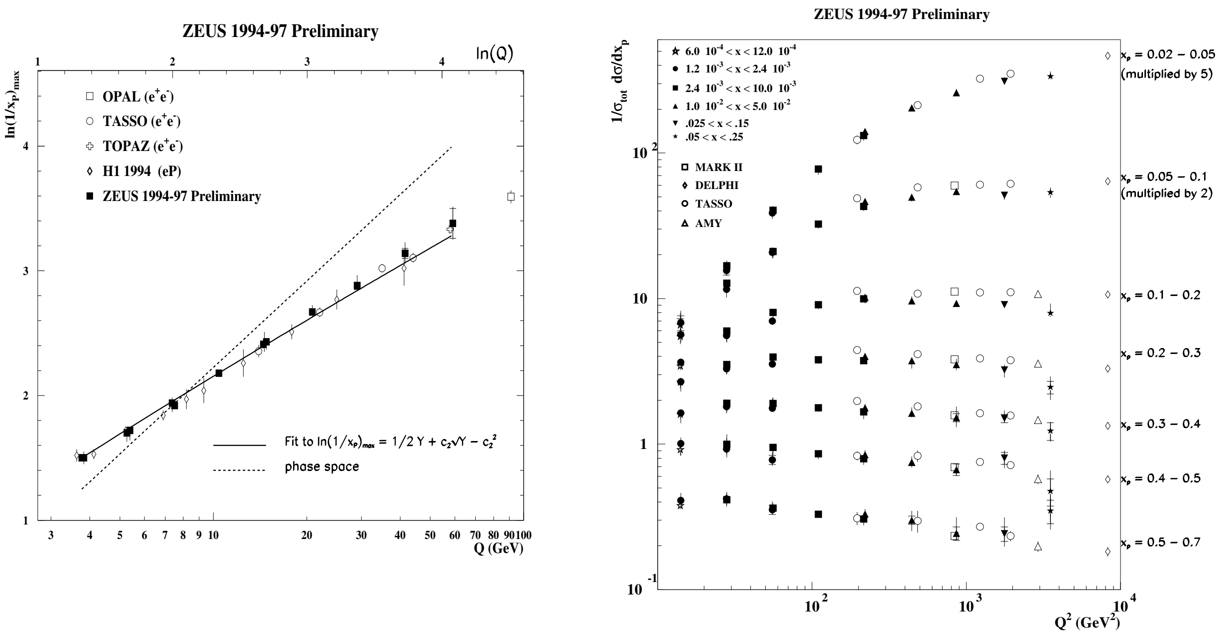

(a) $\ln(1/x_p)_{max}$ versus $\ln(Q)$.

(b) $1/\sigma d\sigma/dx_p$ versus Q^2.

Fig. 11. Charged hadron fragmentation in the current region of the Breit frame.

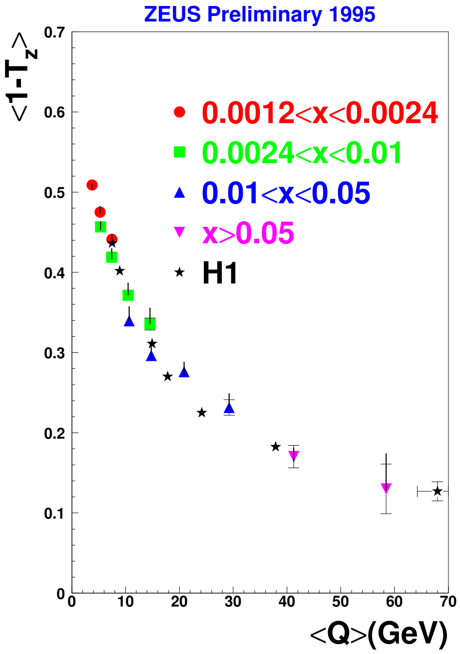

Fig. 12. $<1-T_Z>$ versus Q.

consistent with e^+e^- data (open symbols), but systematically lower at intermediate x_p values. Comparisons with NLO calculations where fragmentation functions extracted from e^+e^- data are implemented can describe the DIS data (see Fig. 2 in[10]). However care needs to be taken to explicitly include strange-quark fragmentation functions which are systematically softer than those of the up/down quarks. This is important since the production of strange quarks from the proton sea in DIS is suppressed (by a factor $\simeq 0.2$) compared to those from e^+e^- annihilation. In order to compare with recent $1/Q^2$ power-correction calculations, the fragmentation function data were also presented as function of $x_{||} = 2p \cdot q/Q^2 = 2p_Z/Q$, where the Z direction is defined by the virtual-photon proton axis. Another approach to investigate the rôle of such power corrections is to sum over these momenta and measure the corresponding thrust distributions $T_Z = 2\Sigma p_Z/\Sigma p$. A series of event shape variables have been measured in the current region of the Breit frame where the power corrections, determined from renormalon calculations, are expected to be characterised by a universal $\overline{\alpha_o}$ and to fall as $1/Q$. In Fig. 12 the measurements using charged tracks in the current region of the Breit frame are displayed as $<1-T_Z>$ versus Q.[11] The characteristic behaviour is in reasonable agreement with published H1 results given at slightly different x values. Other event shape variables are chosen which are relatively insensitive, in varying degrees, to soft gluon emission and collinear parton branchings in order to determine whether a universal $\overline{\alpha_o}$ can be applied. As a first step, comparisons with NLO calculations illustrate the need for additional power correction terms (see Fig. 2 in[11]).

2 Diffraction

The study of diffractive phenomena and their relation to the inclusive cross-section at HERA may hold the key to understanding how a "pomeron" structure emerges from QCD. What we have learned so far is that a single soft pomeron does not describe *all* diffractive data measured at HERA. As the photon virtuality, Q^2, or the vector meson mass increases the cross-sections rise rapidly with increasing W^2. As we investigate the pomeron more closely, a new type of dynamical pomeron may begin to play a rôle whose structure is being measured in DIS. These inclusive diffractive data are consistent with a partonic description of the exchanged object which may be described by perturbative QCD. At this workshop, new results were presented on ϕ electroproduction;[12] the t-dependence of ρ, ϕ and J/ψ photoproduction;[13] $\psi'/J/\psi$ and Υ photoproduction;[14] the determination of $F_2^{D(2)}$ and the diffractive/total cross-section in DIS;[15] diffractive dijet photoproduction cross-sections;[16] event shapes in DIS using the LPS;[17] and, leading baryon production in DIS.[18] These results will help to clarify our understanding of processes which represent a significant fraction, $\sim 10\%$, of the corresponding total cross-sections, yet cannot be understood in terms of a simple hadronisation mechanism.

Vector meson t dependences:[13] Diffraction is characterised by a steeply-falling dependence of the cross-section as a function of t, the momentum transferred at the proton vertex. This characteristic fall-off increases approximately linearly with increasing W. This "shrinkage" behaviour is built into the Donnachie-Landshoff pomeron

$$\alpha(t) = \alpha(0) + \alpha' \cdot t = 1.08 + 0.25 \cdot t.$$

Measurements of the quasi-elastic ($\gamma p \to Vp$) and proton-dissociative ($\gamma p \to VN$) production of vector mesons as a function of t have been performed. The W dependence of the cross-section at fixed values of t allows a direct determination of the exchanged trajectory. In order to gain sufficient range in W and hence constrain α', the ZEUS preliminary results are combined with lower-W elastic measurements and H1 published results. In Fig. 13(a) the ρ^0 trajectory is shown to be a strong function of t with

$$\alpha(t)_{\rho^0} = (1.097 \pm 0.020) + (0.163 \pm 0.035) \cdot t \quad \text{(preliminary)}$$

for the linear fit where the errors are the combined (stat $\oplus$ sys) errors from each experiment. Similarly, the ϕ trajectory (where non-leading Regge trajectories are suppressed due to the Zweig rule) is determined as

$$\alpha(t)_{\phi} = (1.083 \pm 0.010) + (0.180 \pm 0.027) \cdot t \quad \text{(preliminary).}$$

These results are in contrast to the J/ψ trajectory shown in Fig. 13(b) where

$$\alpha(t)_{J/\psi} = (1.175 \pm 0.026) + (-0.015 \pm 0.065) \cdot t \quad \text{(preliminary).}$$

The result for α' is consistent with no shrinkage of the cross-section, which is qualitatively expected from perturbative QCD which allows only a slow (logarithmic) dependence of the trajectory as a function of t. These results herald an era of study where the gluon-dominated QCD structure at the proton vertex is probed using a diffracted heavy flavour probe.

ZEUS 1995 preliminary

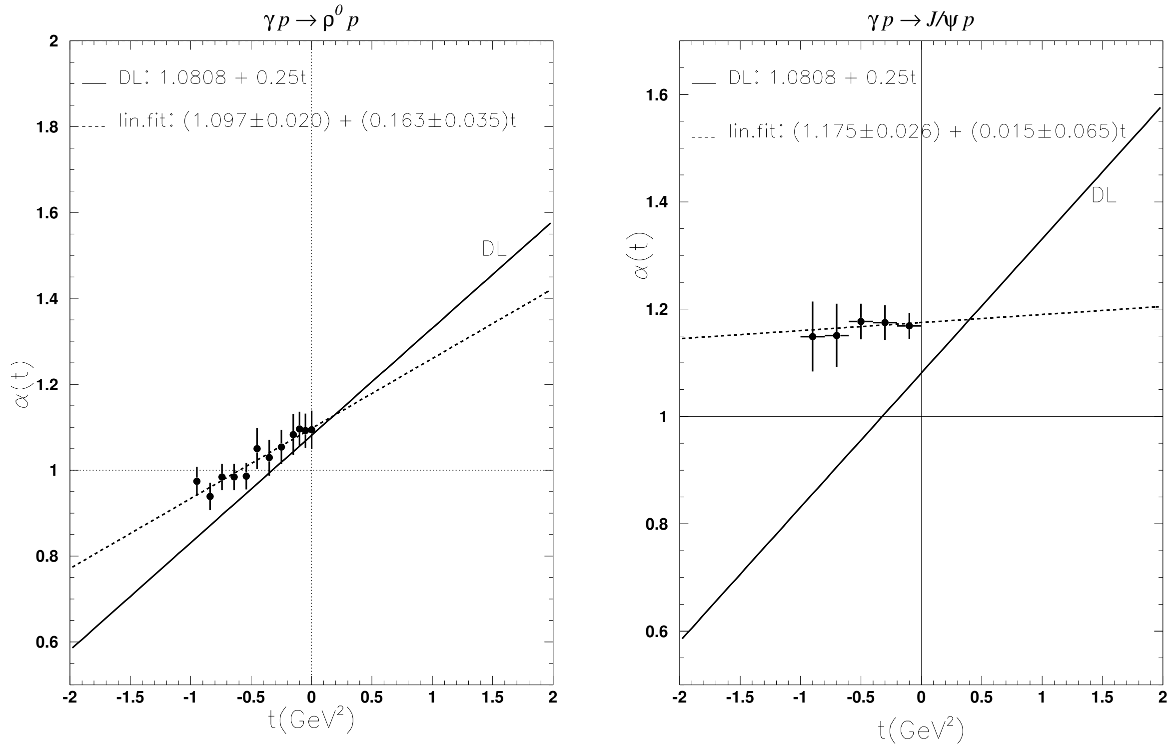

(a) ρ^0 trajectory.

(b) J/ψ trajectory.

Fig. 13. Pomeron trajectories determined from fits to HERA and lower W data.

Higher Mass Vector Mesons:[14] Twenty years after the discovery of the Υ, the first observation of a signal in photoproduction is shown in Fig. 14(a) as a broad enhancement around 10 GeV in the di-muon mass spectrum. The insert in Fig. 14(a) indicates the J/ψ and ψ' resonances: the ψ'/ψ production ratio is measured to be $R = 0.16 \pm 0.02 \pm 0.04$, where the largest contribution to the systematic uncertainty is on the $\psi' \to \mu^+\mu^-$ branching ratio. The result is in agreement with QCD calculations, determined by the wavefunction at the origin for the 1S and 2S states, of $\simeq 0.17$. The observation of the Υ leads to the measurement of the elastic cross-section for the unresolved $\Upsilon(1S)$, $\Upsilon(2S)$ and $\Upsilon(3S)$ states shown in Fig. 14(b). Here the relative rates or muon production from the Υ states is determined from CDF data and applied as a correction to the $\Upsilon(1S)$ calculation. Comparison with the leading-order QCD calculations, where $\sigma_{\text{diff}} \sim xg(x)^2 \otimes \hat{\sigma}$, indicates that the measured cross-section is above these expectations.

ZEUS 1995-97 preliminary

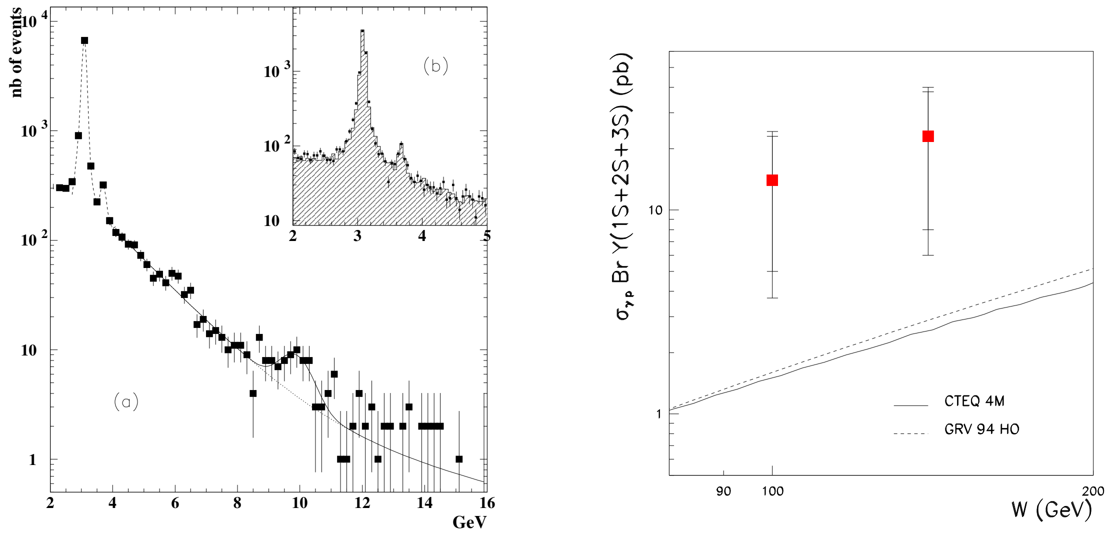

(a) $M_{\mu^+\mu^-}$ spectrum.

(b) Υ cross-section versus W compared to LO calculations.

Fig. 14. Measurement of the elastic Υ photoproduction cross-section.

Diffractive Structure Functions:[15] A new era for diffraction was opened by the observation of large rapidity gap events in DIS and their subsequent analysis in terms of a diffractive cross-section. The diffractive contribution is identified as a non-exponentially suppressed contribution at small masses, M_X, of the dissociating virtual photon system. In Fig. 15 the ratio of this diffractive contribution to the total virtual photon proton cross-section is given as a function of W for various M_X intervals. An approximately constant ratio with W indicates a diffractive contribution which rises with a similar W dependence. This simple observation is contrary to the näive expectation where the diffractive contribution is identified with the forward part of the scattering amplitude and would therefore rise twice as quickly as the total cross-section as a function of W. The rise of the diffractive cross-section with W can be parameterised in terms of a power law, yielding $\alpha_{I\!P}(0) = 1.16 \pm 0.01 \pm 0.02$ (preliminary), after integration over t with a mean exponential slope, $b = 7$ GeV^{-2} and assuming $\alpha' = 0.25$ GeV^{-2}. In order to understand the driving mechanism responsible for this rise, the cross-sections at fixed M_X and W are plotted in terms of scaling variables. Integrating over $x_{I\!P}$, the momentum fraction of the pomeron within the proton, leads to the β dependence of $F_2^{D(2)}(\beta, Q^2)$ ($\equiv F_2^{I\!P}$ specified at $x_{I\!P} = 0.0042$) shown in Fig. 16 where β is the momentum fraction of the struck quark within the pomeron. An approximately flat dependence on β is observed and an approximate scaling in Q^2 emerges from analysis of the data. The decreasing fraction of events in each M_X interval

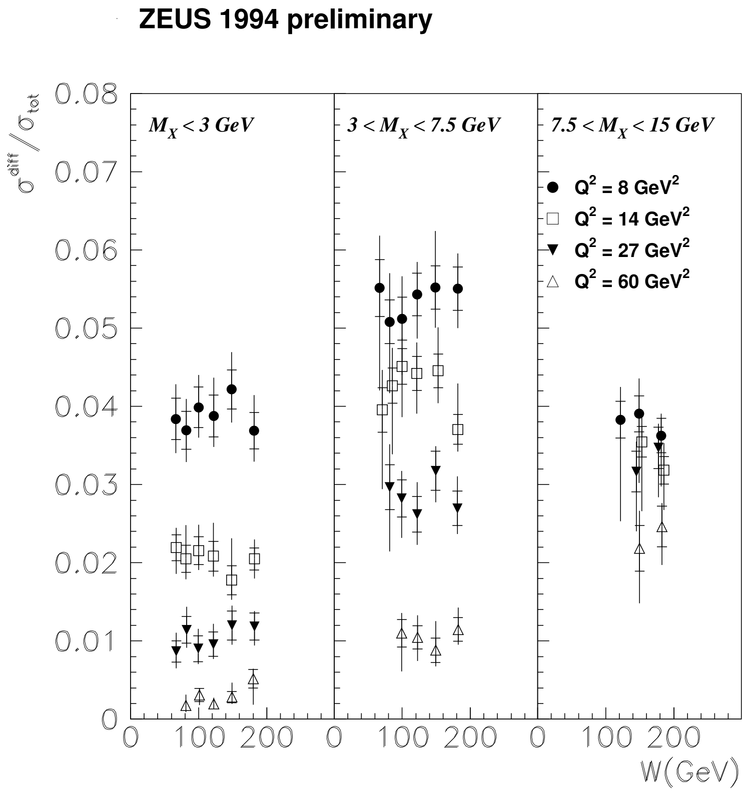

Fig. 15. Diffractive/total cross-section versus W in various M_X ranges.

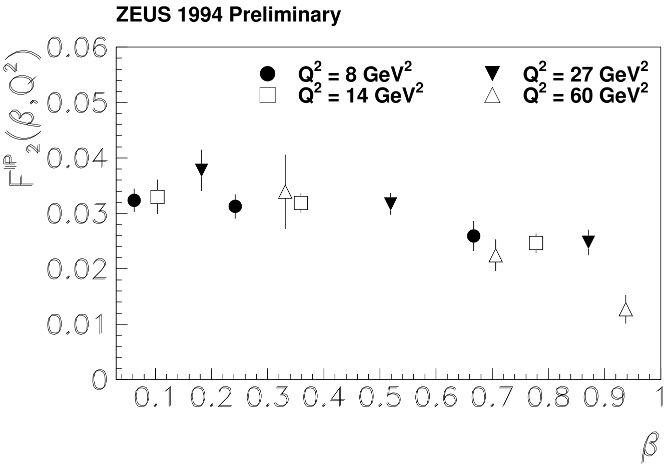

Fig. 16. $F_2^{D(2)}$ versus β.

with increasing Q^2 observed in Fig. 15 can thus be seen as due to integrating over a decreasing $\beta \simeq Q^2/(Q^2 + M_X^2)$ region which is approximately flat in β.

Diffractive Event Shapes:[17] The measurements of the structure function of the pomeron constrain various models of diffraction. These models may be discriminated using event shape variables which are directly sensitive to the underlying partonic structure. Similarly, the data can be directly compared with e^+e^- data where the underlying gluon Bremsstrahlung structure is well known. Tagging a leading proton in the LPS allows a wide range of M_X up to 25 GeV to be explored for $x_{\mathbb{P}} < 0.03$ and $Q^2 > 4$ GeV^2. Measurements of the mean thrust are presented as a function of M_X in Fig. 17. The LPS measurements are able to discriminate amongst various models which assign different partonic structures to the pomeron. The data exhibit reasonably similar values compared to e^+e^- data for all values of M_X suggesting that additional gluon contributions from the pomeron are relatively small. They are also consistent, but systematically higher than, the H1 data obtained using the large rapidity gap method. Improved statistics, from existing data, will help to clarify whether the gluon contribution of the pomeron determined from the scaling violations of $F_2^{D(2)}$[15] is consistent with that extracted from event shape variables[17] and diffractive dijet photoproduction.[16]

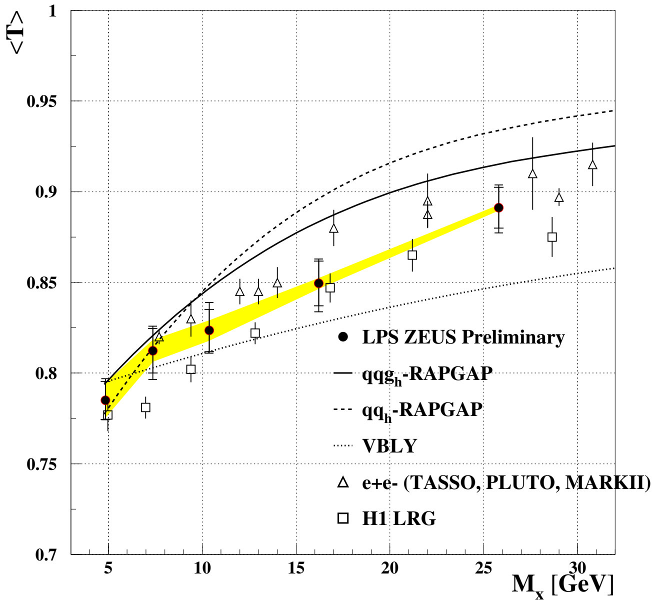

Fig. 17. <Thrust> versus M_X

Leading Baryon Production:[18] Non-diffractive contributions play a rôle at higher values of $x_{\mathbb{P}}$. Measurements of forward proton production allow us to compare data with fragmentation models as well as models based on reggeon exchange. Preliminary results for the corrected rates of proton production in the range $0.60 < x_L \equiv 1 - x_{\mathbb{P}} < 0.91$ for DIS at low and higher Q^2 ($0.1 < Q^2 < 0.8$ GeV^2 and $Q^2 > 4$ GeV^2) are $(13.0 \pm 0.5^{+0.7}_{-0.8})\%$ and $(12.7 \pm 0.3 \pm 0.9)\%$, respectively. The measured rates are typically higher than the currently available fragmentation models by a factor of 1.5 to 2. Measurements of uncorrected forward neutron production rates have been compared to reggeon exchange models: the comparisons indicate that the internal structure of the exchanged reggeon falls like $1 - \beta$ at large β (a dependence similar to π (and higher) Regge exchanges), in contrast to the approximately flat behaviour with β noted earlier for diffractive exchange. The rates for neutron production are approximately the same for DIS, photoproduction and even proton-gas interactions although the W dependence of these cross-sections is significantly different. This suggests that "diquark" fragmentation is a universal process which is to a large extent independent of the type of interaction with the incident proton.

3 High-Q^2 Cross-Sections

The HERA collider provides a unique window to explore *ep* interactions at the highest energies, extending the range of momentum transfer Q^2 by about two orders of magnitude compared to fixed-target experiments. As the HERA luminosity increases we explore the region of $Q^2 \sim 10^4$ GeV^2, where electroweak effects play a rôle. It is in this unexplored kinematic region that we are sensitive to deviations from the standard model (SM). At last year's DIS97 workshop, H1 and ZEUS reported an excess of events compared to the SM predictions from the neutral current (NC) data taken during 1994 to 1996. For the ZEUS analysis the observed rates agreed with expectations except for an excess at the highest Q^2 where two outstanding events with $Q^2 \simeq 40,000$ GeV^2 were observed from a luminosity of 20.1 pb^{-1}. In Fig. 18(a), these events clearly stand out but no new NC outstanding events are observed in the 1997 data, corresponding to a further 26.5 pb^{-1} of data. In Fig. 18(b), one charged current (CC) event is observed at very high $Q^2 \simeq 30,000$ GeV^2 from the 1994-1996 data as well as two further events from 1997 at $Q^2 \simeq 20,000$ GeV^2. The number of events is higher than expectations but is consistent with the standard model. Attention has therefore focussed on measuring the cross-sections at the highest accessible Q^2 values. The theoretical uncertainty on the cross-sections was determined from a ZEUS QCD fit to the structure function data on proton and deuteron targets from SLAC, BCDMS and NMC as well as the neutrino measurements from CCFR, taking into account the correlation amongst the systematic errors of each experiment. $\alpha_S(M_Z^2)$ was varied from 0.113 to 0.123 and a 50% uncertainty in the strange quark content was included. In addition, various published PDFs with different models for charm evolution

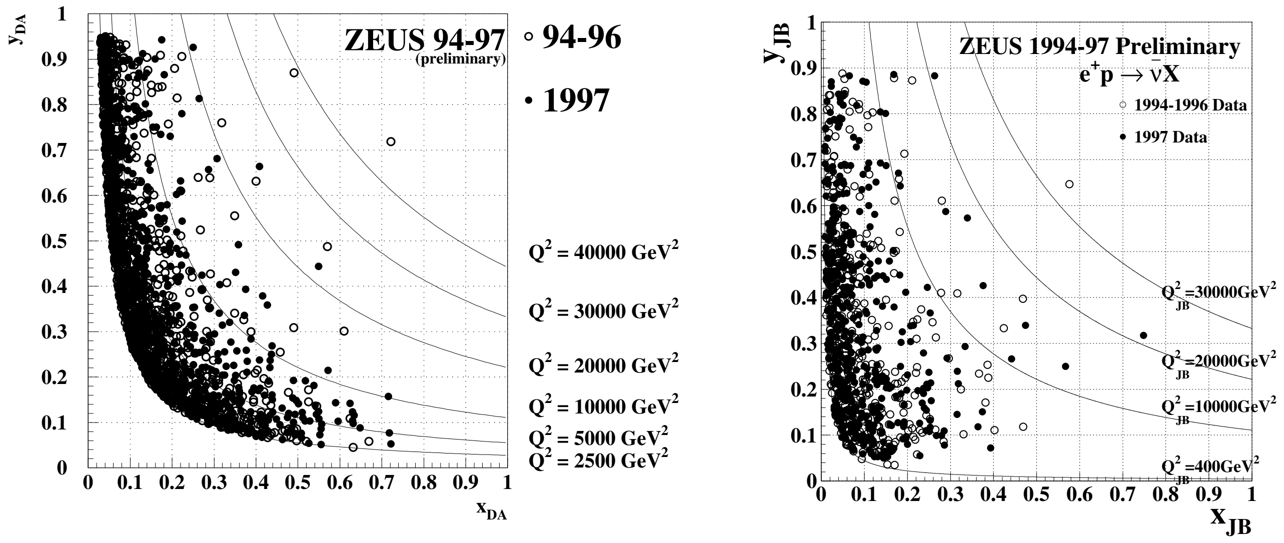

(a) Neutral Current Events.

(b) Charged Current Events.

Fig. 18. Reconstructed y versus x scatter plots for (a) neutral current and (b) charged current events from the 1994-96 (∘) and 1997 (•) data.

were used as well as fits incorporating E706 prompt photon data and CDF jet data. The results yielded SM cross-section uncertainties of $\simeq$ 6-8% on the NC cross-section and $\simeq$ 6-12% on the CC cross-section at the highest accessible Q^2 values. These cross-sections therefore represent a benchmark for the standard model. The cross-sections, discussed below, are corrected to the electroweak Born level and integrated over the complete y range.

Charged Current Cross-Sections:[19] Charged current events are identified by their missing transverse momentum (p_T) due to the escaping neutrino. The cross-section is sensitive to the valence d-quark distribution in the proton:

$$\frac{d^2\sigma_{e^+p}}{dx\,dQ^2} \simeq \frac{G_F^2}{2\pi}\frac{1}{(1+Q^2/M_W^2)^2}[\overline{u}+\overline{c}+(1-y)^2(d+s)].$$

$d\sigma^{CC}/dQ^2$ was measured for $Q^2 > 400$ GeV^2 using the Jacquet-Blondel method where $Q^2_{JB} = p_T^2/1-y_{JB}$, with an RMS resolution on Q^2 of $\simeq$ 25%, reflecting the $35\%/\sqrt{E}$ hadronic energy resolution. 869 events were selected with backgrounds below 2.5%, diminishing with increasing Q^2. The systematic uncertainties, mainly due to the hadronic energy scale uncertainty of ±3%, correspond to $\sim$ 15% uncertainties on the cross-section at lower Q^2 but increase at larger Q^2. In the upper plot of Fig. 19 the cross-section is observed to fall over more than four orders of magnitude. The ratio of the data to the SM, adopting the CTEQ4D PDF, is shown in the lower plot of Fig. 19 where good agreement is observed up to Q^2 of $\simeq$ 10,000 GeV^2. Comparison of the the data uncertainties with those from theory (shaded band) indicates that the data will help to constrain the d-quark densities at large-x. The cross-section is suppressed at lower Q^2, due to the $1/(1+Q^2/M_W^2)^2$ propagator term: this characteristic dependence on Q^2 has been fitted to yield a value for the mass of the exchanged (space-like) W-boson of

$$M_W = 78.6^{+2.5}_{-2.4}(stat.)^{+3.3}_{-3.0}(syst.) \text{ GeV (preliminary)}$$

with an additional PDF uncertainty of ±1.5 GeV.

Photoproduction of W-bosons decaying semi-leptonically has been investigated by searching for events with a high-p_T lepton and missing p_T with 46.6 pb^{-1} of data. This is interesting in the context of the observed excess of high-p_T muons with associated missing p_T observed by H1.[20] In the ZEUS analysis four events are observed in the electron channel where 2.22 ± 0.02 are expected from W production and 1.24 ± 0.35 from various backgrounds. Similarly, zero events are observed in the muon channel where 0.46 ± 0.02 are expected from W production and 0.84 ± 0.23 from other sources. The ZEUS measurements enable 95%CL limits to be set on $\sigma(W)(p_T^{miss} > 20$ GeV) of 2.5 pb and 2.0 pb in the electron and muon channels, respectively.

Neutral Current Cross-Sections:[21] High-Q^2 neutral current events are easily identified from the high-energy scattered positron. The cross-section is particularly sensitive to the valence u-quark distribution in the proton:

$$\frac{d^2\sigma_{e^+p}}{dx\,dQ^2} \simeq \frac{2\pi\alpha^2}{xQ^4}[(1+(1-y^2))F_2(x,Q^2) - (1-(1-y^2))xF_3(x,Q^2)].$$

Here, $F_2 = F_2^{em}(1+\delta_Z)$ is the generalised structure function incorporating $\gamma + Z$ terms which is sensitive to the sum of the quark distributions $(xq + x\overline{q})$ and xF_3 is the parity-violating (Z-contribution) term which is sensitive to the difference of the quark distributions $(xq - x\overline{q})$. $d\sigma^{NC}/dQ^2$ was measured for $Q^2 > 400$ GeV^2 using the double-angle method, with an RMS (σ) resolution on Q^2 of $\simeq$ 5% ($\simeq 2-3$%), and cross-checked using the electron method. Approximately 38,000 events were selected and the systematic uncertainties, resulting from various sources, are typically $\sim 2-3$% at low Q^2 increasing to $\sim$ 10% at higher Q^2. In the upper plot of Fig. 20 the cross-section is observed to fall over more than six orders of magnitude. The ratio of the data to the SM, adopting the CTEQ4D PDF, is shown in the lower plot of Fig. 20 where good agreement is observed up to Q^2 of $\simeq$ 30,000 GeV^2. Comparison of the the data uncertainties with those from theory (shaded band) indicates that the data will constrain the parton densities of the proton at large-x.

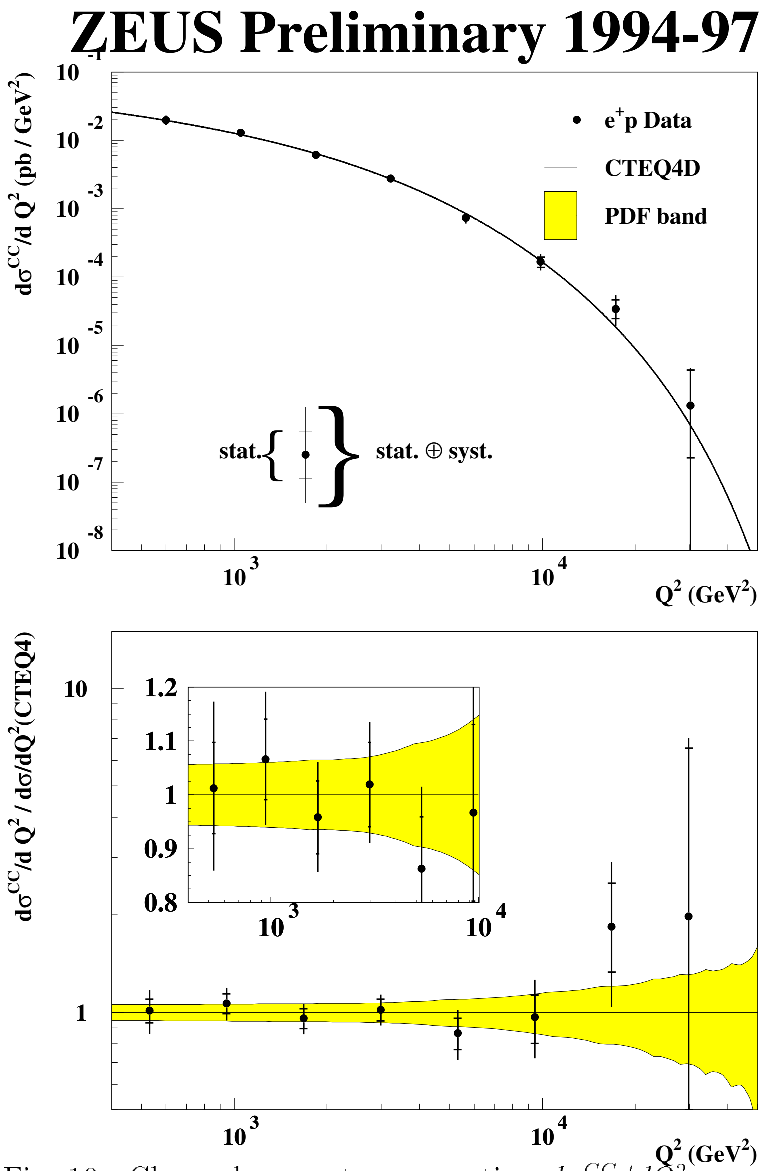

Fig. 19. Charged current cross-section $d\sigma^{CC}/dQ^2$ versus Q^2 for $0 < y < 1$ (upper plot) and ratio with respect to the standard model prediction (lower plot).

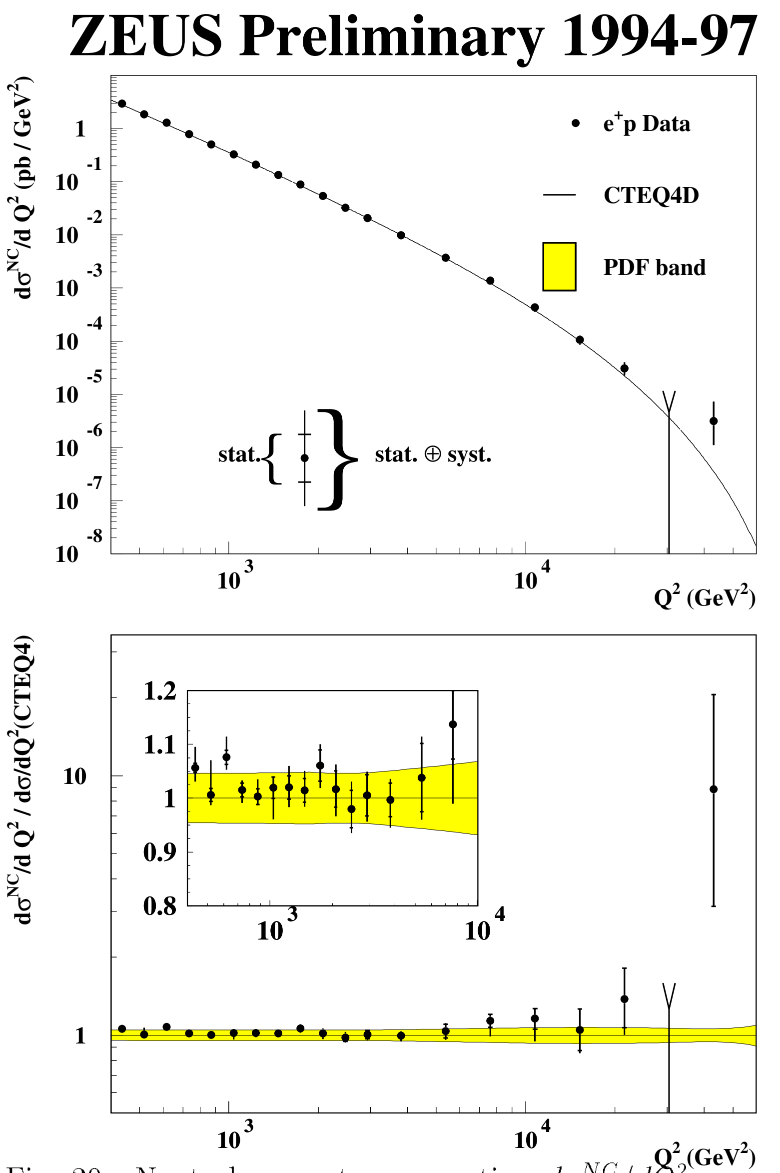

Fig. 20. Neutral current cross-section $d\sigma^{NC}/dQ^2$ versus Q^2 for $0 < y < 1$ (upper plot) and ratio with respect to the standard model prediction (lower plot).

A wide range of new interactions would modify the NC cross-sections in a way which can be parameterised by an effective four-fermion ($eq \to eq$) coupling. Given a convention for the strength of the coupling ($g^2 = 4\pi$), limits can be placed on the effective mass scale (Λ) of these contact interactions. Scalar and tensor terms are constrained by earlier experiments and atomic parity violation experiments provide strong constraints on various vector couplings: the relative size and sign of individual terms in the contact interaction amplitudes is therefore limited to 24 different combinations. These contact interactions all contain a term proportional to $1/\Lambda^4$ which enhances the cross-section as well as a SM interference term proportional to $1/\Lambda^2$ which can either enhance or suppress the cross-section at intermediate Q^2. No significant deviations are found and limits on the 24 models are set in the range of $\Lambda \simeq 2 - 5$ TeV. These limits are competitive with, and in some cases extend, those limits set from from hadronic cross-section measurements at LEP and Drell-Yan electron pair production at the Tevatron.

Conclusions

Selected highlights from the ZEUS analyses of HERA data have been presented. As G. Sterman noted at the DIS97 workshop[22] "We must use the QCD we know well to investigate new physics; but we must also pursue the QCD we do not know well." At the DIS98 workshop a wealth of precise ZEUS data enabled us to identify weak links in our understanding of QCD, to start to probe the electroweak sector and to set limits on physics beyond the standard model.

Acknowledgements

It is a pleasure to thank the organisers for an excellent workshop. Many thanks to the members of the ZEUS collaboration listed below, as well as to Allen Caldwell, Peppe Iacobucci, Alex Prinias, David Saxon and Arnulf Quadt for their help, encouragement, support and advice.

References

[1] J. Vossebeld, DIS98 proceedings (and references therein).

[2] ZEUS Collab., J. Breitweg et al., DESY 98-018.

[3] L. Sinclair, DIS98 proceedings (and references therein).

[4] M. Sutton, DIS98 proceedings (and references therein).

[5] D. Bailey, DIS98 proceedings (and references therein).

[6] B. Surrow, DIS98 proceedings (and references therein).

[7] A. Caldwell, DESY Theory Workshop, Hamburg, September 1997.

[8] M. Riveline, DIS98 proceedings (and references therein);
ZEUS Collab., J. Breitweg et al., DESY 98-050.

[9] M. Martinez, DIS98 proceedings (and references therein);
ZEUS Collab., J. Breitweg et al., DESY 98-038.

[10] J. Okrasiński, DIS98 proceedings (and references therein).

[11] R. Waugh, DIS98 proceedings (and references therein).

[12] S. Kananov, DIS98 proceedings (and references therein).

[13] T. Monteiro, DIS98 proceedings (and references therein).

[14] A. Bruni, DIS98 proceedings (and references therein).

[15] H. Kowalski, DIS98 proceedings (and references therein).

[16] ZEUS Collab., J. Breitweg et al., DESY 98-045.

[17] R. Wichmann, DIS98 proceedings (and references therein).

[18] A. Garfagnini, DIS98 proceedings (and references therein).

[19] G. Howell, DIS98 proceedings (and references therein).

[20] T. Greenshaw, DIS98 proceedings (and references therein).

[21] D. Williams, DIS98 proceedings (and references therein).

[22] G. Sterman, AIP conference proceedings 407, ed. J. Repond and D. Krakauer, 243.